Correspondence to:
M. Sakradzija,
mirjana.sakradzija@mpimet.mpg.de

Physically Constrained Stochastic Shallow Convection in Realistic Kilometer-Scale Simulations

Mirjana Sakradzija[1,2] (ID) and **Daniel Klocke**[2,3] (ID)

[1] Max Planck Institute for Meteorology, Hamburg, Germany, [2] Hans-Ertel-Zentrum für Wetterforschung, Offenbach am Main, Germany, [3] Deutscher Wetterdienst, Offenbach am Main, Germany

Abstract A new configuration of a parameterization for shallow convection in the Icosahedral Nonhydrostatic Model (ICON) is described and tested on a single realistic test case. As a test case, a shallow convective day over Germany is simulated using four different configurations of ICON. These configurations differ by the choice of the shallow convection parameterization, which can be deterministic, stochastic, or completely switched off. As the fourth configuration, the ICON large eddy simulation setup is used as a reference against which the three other ICON model configurations are tested and compared at resolutions from 1 to 10 km. It is demonstrated that a deterministic mass flux closure combined with the stochastic sampling of the cloud base mass fluxes corrects the spatial and temporal distribution of cloudiness. The mean vertical structure of the cloud layer and vertical profiles of the thermodynamic variables in the boundary layer are also improved. The stochastic parameterization adapts to the model resolution by its formulation, while a limited scale-aware behavior is present in the outcome of the simulations. This limitation stems from the resolution dependence of the resolved dynamics, which produces incorrect distributions of cloudiness, and scale-dependence opposite of what is expected based on the reference large eddy simulation results. The deterministic version of the convection scheme cannot correct the behavior of the resolved dynamics, while the stochastic version corrects the resolved dynamics to some extent and improves the overall behavior across resolutions.

1. Introduction

The main task of a cumulus parameterization is to represent the interaction between the subgrid-scale processes and the resolved dynamical processes by transporting heat and moisture vertically in the atmospheric model column. Over the time this scope widened, especially with an increase of the model resolution to kilometer scales, and the requirements for an adequate representation of convection raised to cover more processes and interactions. These include the vertical mass transport and water phase changes, interactions with radiation, interactions with the boundary layer, the mechanical interactions with the mean flow, and representation of nondeterministic and nondiagnostic effects (Arakawa, 2004). To achieve these objectives, an integrated and holistic approach to modeling of convection has to be undertaken. Moreover, at the kilometer-scale resolutions, the task of modeling of convective flows is threefold. First, convection requires a subgrid formulation that takes into account the high resolution of the model grid. Second, some convective scales are picked up by the model dynamics but are not properly resolved, so they need to be corrected. And third, there is a need for an adequate coupling between the subgrid and resolved convective flows. In this paper, we present a first attempt to include nondeterministic and nondiagnostic effects of the boundary layer convection in a realistic case by focusing on all three mentioned tasks of modeling at the convective scales.

The first task when modeling shallow convection on high-resolution grids is to formulate the subgrid ensemble of convective clouds and to correctly represent the statistical cloud samples in the gray zone regime. This is a regime between adequately resolved shallow convection O(10 m) and coarser resolutions of O(10 km), where convection can, in principle, be adequately parameterized (e.g., Hong & Dudhia, 2012). In the gray zone, the average properties of an ensemble of shallow convective clouds or other coherent structures of interest are not representative of a single-point subgrid state. This was previously recognized by Craig and Cohen (2006) in the case of deep convection. They developed and tested a theory of fluctuations of convective states around the ensemble average state relying on the theory of equilibrium statistical ensembles. For shallow convection, Dorrestijn et al. (2013) recognized the resolutions from 50 m to 10 km as the scales at

which a stochastic parameterization of the boundary layer turbulent fluxes is needed. By using a similar consideration of stochastic scales, Sakradzija et al. (2015) developed a stochastic parameterization of the cloud base mass flux in shallow convection following the work of Craig and Cohen (2006). This is a scale-aware method by which fluctuations about the ensemble average subgrid convective state increase with model resolution so that the distribution of the possible convective states changes from a normal-like distribution on the coarse grids toward a long-tailed distribution at high-resolutions given identical large-scale conditions. In the subsequent work of Sakradzija et al. (2016) a step further was made and the parameterization developed in Sakradzija et al. (2015) was coupled with a version of the Eddy-Diffusivity Mass Flux parameterization (EDMF; Neggers et al., 2009; Siebesma et al., 2007) in the Icosahedral Nonhydrostatic (ICON) model and tested in an idealized convective case. It turned out that off-line development and testing of a parameterization is not by itself sufficient as a proof of a concept for a parameterization. It is crucial to study the coupling and the interaction of the subgrid stochastic parameterization with resolved convective circulations in the gray zone (Sakradzija et al., 2016).

The convective circulations in the gray zone are not properly resolved, as the spatial scales and the intensity of circulations are artificially set by the model resolution instead of being controlled by the physical processes in the boundary layer (Zhou et al., 2014). In addition, these circulations often organize into spurious patterns under undisturbed conditions (Ching et al., 2014; LeMone et al., 2010; Piotrowski et al., 2009; Sakradzija et al., 2016; Zhou et al., 2014). This could cause localized biases in the representation of the boundary layer clouds, precipitation, and the atmospheric radiative transfer. Several methods were proposed to suppress the underresolved convective circulations and their spurious features in the gray zone regime (Ching et al., 2014; Takemi & Rotunno, 2003). By these methods spurious circulations can be suppressed by tuning the parameters of the boundary layer parameterization; however, such an approach is resolution dependent and requires retuning with each change in the model setup (Ching et al., 2014; Takemi & Rotunno, 2003). Furthermore, realistic convective features are suppressed altogether with the spurious ones, so the benefits from running a model on high resolution are reduced to the effects of the high-resolution boundary data, such as orography or land use data. Another solution to the underresolved convective circulations would be to modify and correct them in some aspects. For example, the observed spurious organization patterns can be removed by introducing stochastic perturbations, while still retaining a convective circulation regime, such as in Sakradzija et al. (2016). In an example of an idealized case over the ocean modeled in ICON, the stochastic perturbations invigorate the resolved part of the convective circulations and change their spatial patterns to resemble more closely the coarse-grained fields resulting from a large eddy simulation (LES; Sakradzija et al., 2016). In this paper, we also examine to what extent and in which aspects are the underresolved circulations and their organization regimes changed by using a stochastic parameterization.

The task of modeling shallow convection in the gray zone also has a more technical aspect as a task of choosing the proper scales at which to apply the forcing to the parameterization. The conventional approach to couple a parameterization to the model dynamics is to force the subgrid scales using the local grid point values of the prognostic variables. However, the local values as an input to the parameterization are corrupted by the underresolved dynamics in the gray zone. Such local input can be interpreted as noise that further gets amplified by the subgrid processes, so that a small amplitude noise in the input at convective scales results in large-amplitude noise as a parameterization output at the same scales (Lander & Hoskins, 1997). Therefore, it would be desirable to apply the forcing to a parameterization in the gray zone at the *believable* scales, a term coined by Lander and Hoskins (1997), which are represented by a correct energy level on a given scale. This could be achieved by averaging or filtering the input fields to a parameterization, as done in the parameterization of Plant and Craig (2008) applied to deep convection. Here we use a similar method of averaging the input to the parameterization that was previously applied to shallow convection in the gray zone by Sakradzija et al. (2016).

In operational numerical weather forecasts and climate projections, stochastic parameterizations are used to represent uncertainty in ensemble simulations (Berner et al., 2009), but also to improve the mean state of the model climate (Palmer, 2001). To achieve this, two fundamentally different approaches are taken. In the first approach, stochastic perturbations are introduced by patterns, which cover larger spatial and temporal scales. Here the connection to physical processes is not direct, but perturbations represent the larger scale effect of physics uncertainties via the coupling to the dynamics on larger scales. The perturbations on the large scale will affect the small scales and subsequently propagate back upscale as if they had simply originated in the small scales. In the second approach, certain physical processes are perturbed locally and the perturbations

Table 1
ICON Model Resolution and Time Steps

Equivalent resolution (km)	Edge length (km)	Cell area (km^2)	Time step (s) (def./stoch.)
1.2	1.9	1.56	10
2.5	3.8	6.24	20/12
5	7.6	24.94	40/30
10	15.2	99.77	80/60

Note. The time steps used in the default (def.) and stochastic version of convection (stoch) have different values. ICON = icosahedral nonhydrostatic model.

propagate upscale to have a significant impact on the simulation. In the end there may be no way to distinguish if an error originated on the small or large scales, and both approaches will lead to comparable results (Durran & Weyn, 2016). Disturbing physical parameterizations directly is attractive, because we can understand model errors before they interacted (Klocke & Rodwell, 2014) and can control them in a physical-process constrained way.

The goal of this paper is to represent the local fluctuations of subgrid shallow convection and thus to improve the temporal and spatial variability of shallow convection. In addition, due to the scale-aware formulation of the stochastic parameterization, we expect to improve the distribution of cloudiness across the kilometer-scale resolutions. The scale-aware behavior should be reflected by changing the shape of the distributions of cloud properties depending on the model resolution, but it should also retain the large-scale thermodynamic state that stays similar across different resolutions. To achieve this, the stochastic sampling has to be constrained by some physical principle that will impose the controls on the parameters of the sampling distributions (see section 2.2.2).

In the following, we describe the formulation and coupling of the stochastic parameterization of shallow convection in ICON (section 2). In section 3 we test three ICON configurations that differ by the choice of the representation of shallow convection, which can be deterministic, stochastic, and completely switched off. The tests are conducted at four different model resolutions spanning from 1 to 10 km to assess the resolution dependency of the simulation outcome. The resolved convective circulations and the effects of the stochastic perturbations on the resolved convective regime are studied in section 3.5. Tests of sensitivity to several model parameters are conducted in section 3.6, and overall conclusions are given in section 4.

2. Model Description

2.1. ICON Model

All simulations in this study are performed using the Icosahedral Nonhydrostatic general circulation Model (ICON) developed by the German Weather Service (DWD) and the Max Plank Institute for Meteorology (MPI-M) (Zängl et al., 2015). The model solves the nonhydrostatic equations using an icosahedral triangular Arakawa C grid. The prognostic variables are the horizontal velocity component normal to the triangle edges v_n, the vertical wind component w, virtual potential temperature θ_v and due to the requirement for the mass conservation, a flux form continuity equation is solved for the Exner pressure, Π. The equations are discretized using a two-time-level predictor-corrector scheme (Zängl et al., 2015). As the basis for the kilometer-scale simulations in this paper, we used the default numerical weather prediction (NWP) physics package that is used operationally at DWD (Zängl et al., 2015), with an exception of the parameterization of deep convection, which we do not use on the kilometer-scale resolutions. The simulations are set up at four different resolutions (see Table 1) using three different configurations of ICON. These configurations differ by the choice for the representation of shallow convection, which can be the deterministic Tiedtke-Bechtold parameterization (Bechtold et al., 2014), a stochastic version of the Tiedtke-Bechtold parameterization developed in this study or no subgrid parameterization of shallow convection.

A LES of a shallow convective day in Germany and neighboring regions, 5 May 2013, is conducted using the ICON configuration developed for the large eddy simulations (ICON-LES; Dipankar et al., 2015). This test case is one of the several cases defined in the High Definition Clouds and Precipitation for advancing Climate Prediction (HD(CP)^2) project with a purpose of developing, testing, and evaluating the ICON-LES (Heinze et al., 2017). The LES configuration of ICON uses the same dynamical core as the general circulation ICON model, with a difference in the treatment of the subgrid processes. In difference to the NWP physics package, the
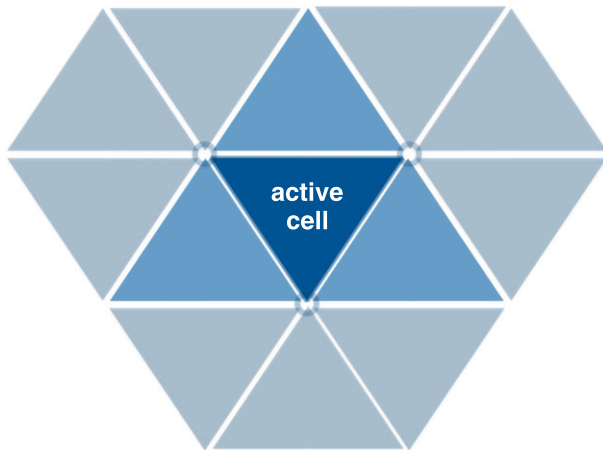
Figure 1. A sketch demonstrating the averaging choice over the two levels of the neighboring cells.

ICON-LES parameterization package includes the 3-D turbulence scheme based on the Smagorinsky scheme, a double-moment microphysics scheme based on Seifert and Beheng (2006) and a simple all-or-nothing (0 or 1) scheme for the cloud cover (Sommeria & Deardorff, 1977). For more details about the ICON-LES, see Dipankar et al. (2015).

2.2. Stochastic Routine as an Add-on to Shallow Convection

The parameterization of shallow convection in ICON is a version of the Tiedtke (1989) shallow convection parameterization. It is a bulk representation of convection that includes plume model equations and a bulk mass flux closure based on the boundary layer moist static energy convergence as described in Bechtold et al. (2014). The occurrence of shallow convection in a model grid column is decided by an ascending test parcel forced by the surface properties. The grid column is recognized as shallow convective if the test parcel reaches the lifting condensation level having a positive vertical velocity at that level and if the thickness of the cloud layer is less than 200 hPa. Otherwise, convection is not parameterized. The regions occupied with deep convection are explicitly modeled in the current model setup for the kilometer-scale resolutions.

The stochastic routine used in the present study is developed from the version of the routine that was previously applied in Sakradzija et al. (2016), where it was coupled to the Eddy-Diffusivity Mass-Flux (EDMF) scheme (Siebesma et al., 2007). In the following, we focus on the novelties in the formulation of the stochastic parameterization and we refer the reader to Sakradzija et al. (2015, 2016) for more details about the stochastic sampling.

The bulk mass flux closure is based on the statistical quasi-equilibrium assumption, which is not valid on kilometer-scale grids. Based on the LES coarse-graining studies (Dorrestijn et al., 2013; Sakradzija et al., 2015) quasi-equilibrium can be applied to shallow convection at the scales of around 20 km and coarser. Therefore, we apply the bulk mass flux closure at such larger scales. The averaging is done over the neighboring grid cells of each active cell in ICON (Figure 1). At present, two levels of averaging are available in ICON, the first level covers the active cell and the three neighboring cells of the triangle edges, while the second level covers the active cell and the 12 vertex neighboring cells (see Table 2). Here we use the second level of averaging, which results in different areas of averaging for different resolutions. We test in section 3.6 the effects of this choice on the simulation results.

When the bulk mass flux closure is applied over a larger area around a grid cell, the bulk mass flux M_{bulk} can be interpreted as equivalent to the ensemble average total mass flux $\langle M \rangle$ of a cloud statistical ensemble as in Plant and Craig (2008) and Sakradzija et al. (2016). $\langle M \rangle$ is the expected value of the ensemble distribution $p(M)$, which is the distribution of the possible values of the total mass flux within the grid column.

2.2.1. Random Sampling of the Cloud Number and Mass Flux

In the stochastic scheme, different realizations of the subgrid shallow convective mass flux within model grid columns, M, are randomly sampled from the ensemble distribution, $p(M)$ (Figure 2). The analytic form of $p(M)$ is not available, and that is why the sampling of M is implemented in two steps, as described in

Table 2
ICON Model Resolutions and Areas of the Averaging Regions

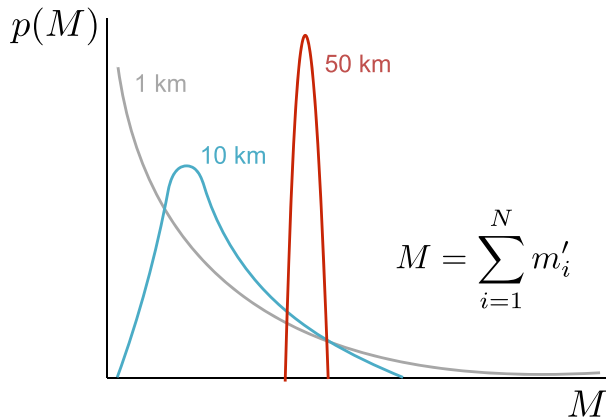| Equivalent resolution (km)	Cell area (km^2)	Area of the (1) level of averaging (km^2)	Area of the (2) level of averaging (km^2)
1.2	1.56	6.24	20.28
2.5	6.24	24.94	81.07
5	24.94	99.76	324.22
10	99.77	399.08	1297.06

Figure 2. A sketch of the total mass flux distribution $p(M)$ and its dependency on the model resolution.

Sakradzija et al. (2015). First, a number of new clouds, n, is initialized in each grid column by randomly sampling the Poisson distribution:

$$p(n) = \frac{\left(G\Delta tA_{\text{cell}}\right)^n e^{-G\Delta tA_{\text{cell}}}}{n!} \tag{1}$$

where $G\Delta tA_{\text{cell}}$ is the cloud-generating rate per model time step and per grid cell. Second, for each new cloud the lifetime average mass flux, m, is randomly sampled from a bimodal Weibull distribution:

$$p(m) = \sum_{j=1,2} f_j \frac{k_j}{\lambda_j} \left(\frac{m_j}{\lambda_j}\right)^{k_j-1} e^{-(m_j/\lambda_j)^{k_j}} \tag{2}$$

where λ and k are the scale and the shape parameters of the Weibull distribution, f is the fraction of cloud number that constitutes each distribution mode, and index j denotes the distribution mode. Two modes of the Weibull distribution are used in the stochastic routine, one to represent forced and passive clouds (f_1) and the second one to represent the active cumulus clouds (f_2). The two modes are sampled using the same routines, so in the following we will drop the index j from the notation.

The sampling of the Poisson distribution for the cloud number, n, is done following the procedure developed in Ahrens and Dieter (1982). By this procedure, if the cloud-generating rate is $G \geq 10$ the random Poisson samples are generated by sampling a normal distribution and applying a correction as in Ahrens and Dieter (1982). For $G < 10$ an inversion method of the Poisson distribution function is used, see the table in Ahrens and Dieter (1982). The code for randomly sampling the Poisson distribution is written by Miller (2000).

The sampling of the cloud base mass flux from the Weibull distribution is done by using an inversion of the Weibull cumulative distribution function as in Sakradzija et al. (2015). The inverse cumulative Weibull distribution function is given by

$$m = \lambda \left(-\log(1-p)\right)^{1/k} \tag{3}$$

A random number p is generated assuming a uniform distribution.

2.2.2. Cloud Lifetimes

The Weibull distribution (equation (2)) is used to describe $p(m)$ in order to introduce the dependency of the cloud mass flux to its lifetime, which is the main reason for deviations from the exponential distribution function (Sakradzija et al., 2015). In the stochastic sampling routine, a number of new clouds, n, is initialized at each time step and for each new cloud the average mass flux, m, is sampled from $p(m)$. The instantaneous mass flux of each cloud m' is recovered during the simulation from the lifetime average mass flux m by assigning a life cycle to each cloud (see Figure 3 and Sakradzija et al., 2015). As a result of this, at each time step a grid column holds a number of old clouds, n_{old}, and a number of new clouds, n, all in different stages of their life cycles. It is desirable to represent the life cycles of clouds in the model in order to reproduce the correct variability of M and to keep the consistency in the model formulation (see Sakradzija et al., 2015). In Sakradzija et al. (2015) it was demonstrated that a correct variability of the subgrid mass flux will be reproduced only if the Weibull distribution function is introduced in the stochastic routine along with the explicit cloud life cycles. Another very important role of the life cycles is that they introduce memory into the parameterization of clouds.

2.2.3. Calculation of the Total Mass Flux Distribution $p(M)$

After the new clouds are sampled and added to the grid column, the total mass flux is the sum of the instantaneous mass fluxes of all the existing clouds in that grid column:

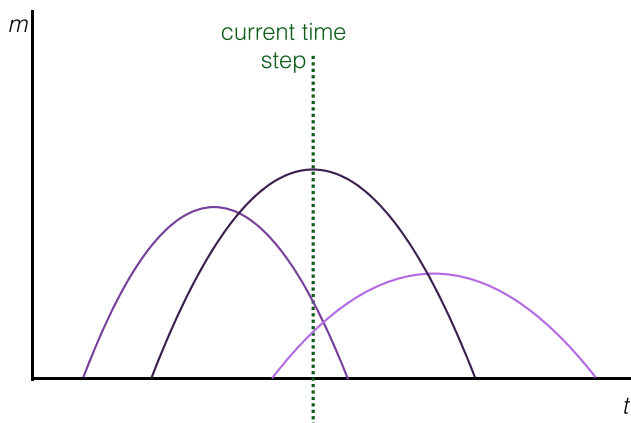$$M = \sum_{i=1,N} m'_i \tag{4}$$

Figure 3. A sketch of the cloud life cycles. Three clouds are present in the active grid cell, the first one near the end of its life cycle, the second at the peak, and the third at the beginning of its life cycle.

N is the sum of the number of the already existing old clouds in the column still remaining from the previous time steps, n_{old}, and the newly initiated

Table 3
List of the Parameters Used in the Stochastic Routine and Their Default Values

Parameter	Description	Value	Unit
α	fitting parameter in the lifetime relation	0.33	s^2/kg
β	fitting parameter in the lifetime relation	0.8	-
k	shape parameter of Weibull distribution	0.8	-
$\langle m_1 \rangle$	average mass flux of passive clouds	50,000	kg/s
C_1	minimum average mass flux of active clouds	78,643.2	kg/s
C_2	fitting parameter	0.13	-
f_2	fraction of active clouds	60	%

clouds, n. Prime ′ indicates the instantaneous value of mass flux in difference to the lifetime average m. Thus, $p(M)$ is a convolution of two distributions, the distribution of the total number of clouds in a model grid column N, and the distribution of the instantaneous cloud base mass flux m' of each individual cloud that exists in the grid column at that time step. $p(M)$ is a scale-aware distribution as it takes various shapes depending on the model resolution (Craig & Cohen, 2006; Sakradzija et al., 2015). This change in the shape is dictated by the average number of clouds in the model grid column. On the coarse grids a grid cell can contain a large number of clouds, and fluctuations of the possible realizations of the total mass flux in the given grid column will be small. This is a result of the law of large numbers, which implies the shape of $p(M)$ to be a narrow symmetric distribution. As the average number of clouds in a model column decreases, which is imposed by increasing resolution, the fluctuations of M also increase and p(M) approaches the form of p(m).Thus, $p(M)$ takes various shapes covering a spectrum from a bell-shaped distribution at coarse resolutions to a long-tailed distribution on the high-resolution grids (Figure 2). This change in the shape of $p(M)$ comes through $G\Delta t A_{cell}$ which is a number of new clouds to be initialized during the time step Δt in a grid cell area A_{cell}.

The sampling distribution (equation (2)) is defined for the lifetime average values of the mass flux of individual clouds, m, while $\langle M \rangle$ is an instantaneous quantity. The bulk mass flux M_{bulk}, taken as equivalent to $\langle M \rangle$, can be related to the parameters of the sampling distributions (equations (1) and (2)). This can be done by integrating the ensemble average instantaneous mass flux distribution defined as $\langle p(m') \rangle = \langle \tau(m) \rangle \langle G p(m) \rangle$ as in Sakradzija et al. (2015):

$$\langle M \rangle = \int_0^\infty m \langle \tau(m) \rangle \langle G p(m) \rangle \mathrm{d}m \tag{5}$$

which results in

$$\langle M \rangle = G \alpha \lambda^{k+1} \Gamma \left(2 + \frac{1}{k} \right) \tag{6}$$

(Sakradzija et al., 2015). The $\tau(m)$ is the cloud lifetime as a function of the cloud mass flux, and α is one of the fitting coefficients of the cloud lifetime relation $\tau = \alpha m^\beta$, which is based on LES (see Table 3 and Sakradzija et al., 2015). G is the weighting factor of $p(m)$, called the cloud-generating rate (Sakradzija et al., 2015). It is defined as a number of clouds initialized in one second per square meter. The shape parameter of the Weibull distribution, k, is considered as a universal constant, $k = 0.8$, and is assumed to be equal to the β exponent of the lifetime relation based on the LES study of Sakradzija and Hohenegger (2017). The number of parameters is thus reduced by one, which leaves the two remaining unknown parameters that require closure, G and λ.

2.2.4. Closure of the System
The two unknown parameters G and λ of the two sampling processes that are described by equations 1 and 2 can be substituted by quantities that are physically more intuitive, the bulk mass flux, $M_{bulk} \sim \langle M \rangle$ (equation (6)), and the average mass flux per cloud, $\langle m \rangle$, as the expected value of the Weibull distribution:

$$\langle m \rangle = \lambda \Gamma(1 + 1/k) \tag{7}$$

for each of the two modes.

Thus, the two sampling processes can be described using the two equations, (6) and (7), which require a closure for the two unknown parameters, $\langle M \rangle$ and $\langle m \rangle$. The first physical constraint of this closure is based on the bulk mass flux M_{bulk} that results from the deterministic Tiedtke-Bechtold scheme. This closure is based on the balance between convection and the mean advection and other physical processes in the boundary
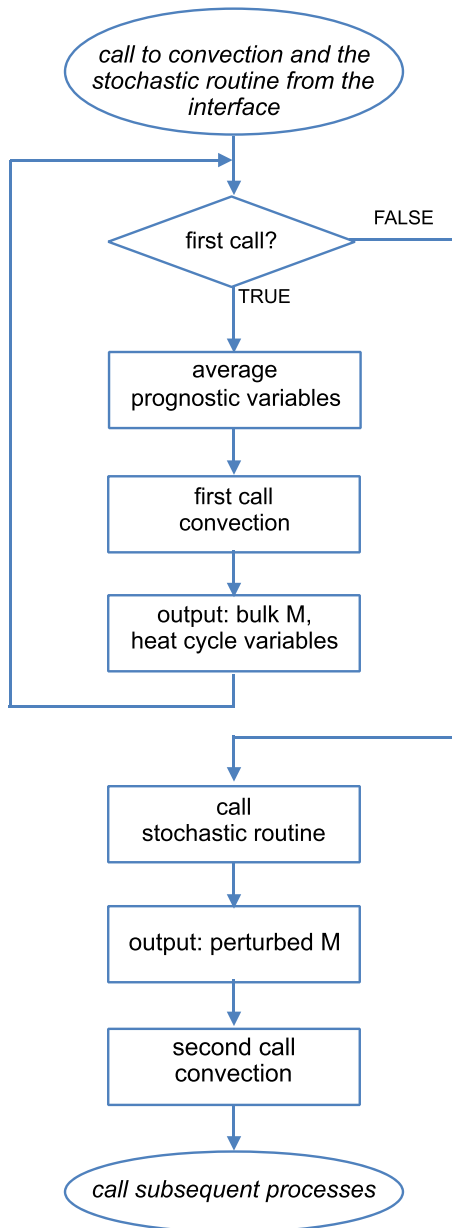
layer (PBL) represented by the vertically integrated tendency of the moist static energy, h, between surface (sfc) and cloud base (cb) (Bechtold et al., 2014):

$$\langle M \rangle \sim M_{\text{bulk}} = \left(-\frac{1}{g} \int_{p_{\text{sfc}}}^{p_{\text{cb}}} \frac{\partial \overline{h}}{\partial t} dp \right) / (\Delta h) \qquad (8)$$

or in a simpler form

$$\langle M \rangle \sim \frac{h_{\text{PBL}}}{\Delta h} \qquad (9)$$

The second constraint is based on the study of Sakradzija and Hohenegger (2017) in which the average mass flux per cloud is related to the efficiency of the convective heat cycle, η, and the ratio of the total surface turbulent heat fluxes, F_{sfc}, and the excess of the moist static energy within the updrafts in respect to the environment at the cloud base level, Δh:

$$\langle m \rangle = C_1 + C_2 \eta \frac{F_{\text{sfc}}}{\Delta h} \qquad (10)$$

C_1 and C_2 are the fitting parameters based on LES (Table 3). The equations (9) and (10) are the two physical constraints that determine the sampling distributions in the stochastic routine and are a novelty compared to the previous version of the stochastic routine in Sakradzija et al. (2016). The physical constraint, equation (10), replaces the use of the average lifetime per cloud that was fixed to 10 min in the previous version of the stochastic routine.

2.2.5. Coupling of the Stochastic Routine With Shallow Convection

The stochastic routine is a separate module in the ICON model that is called from the model interface between subgrid processes and dynamics. The coupling procedure is similar to the coupling of the previous version of the stochastic routine in Sakradzija et al. (2016). The time line of the calls to convection scheme and the stochastic routine (Figure 4) starts with the averaging of the input prognostic variables to the Tiedtke-Bechtold shallow convection. The averaging is done over the neighboring grid cells that share the three vertices of the active triangle cell, which makes 13 cells in total (cf. Figure 1). The area of the averaging is thus different for different resolutions (see Table 2). The averaged prognostic variables are then used to force the convection scheme, the bulk mass flux M_{bulk} is calculated and passed to the interface level. The variables necessary for the calculation of the average mass flux per cloud $\langle m \rangle$ based on the heat cycle formalism (equation (10)) are also output after the first call of the shallow convection scheme.

Figure 4. A simplified code algorithm: The calling sequence of the stochastic extension to the shallow convection scheme.

After the first call to convection, the stochastic routine is called and forced by M_{bulk} and other variables necessary for the calculation of $\langle m \rangle$. The perturbed mass flux in the active grid cell, M, is produced by the stochastic routine and used as an input to the second call of the shallow convection scheme. In the second call, the convection parameterization continues from the point of the mass flux closure, but using the perturbed mass flux M in the plume budget equations and subsequent calculations, instead of the bulk mass flux M_{bulk}.

In the stochastic setup, the Tiedtke-Bechtold scheme is retained in its original form as in Bechtold et al. (2014), except for the deactivation of the mass flux safety limiters and the controls of the shallow convection activity. The deterministic version still retains the safety limiters of the mass flux. These limiters are used to prevent very high mass flux values that can cause instabilities in the resolved flow and disruption of the model run. These safety limiters are deactivated in the stochastic version of the scheme to allow the stochastic process to change the temporal and spatial variability. We suspect that the safety limiters might not be necessary in the stochastic version of the convection parameterization because of the higher probability of low mass flux
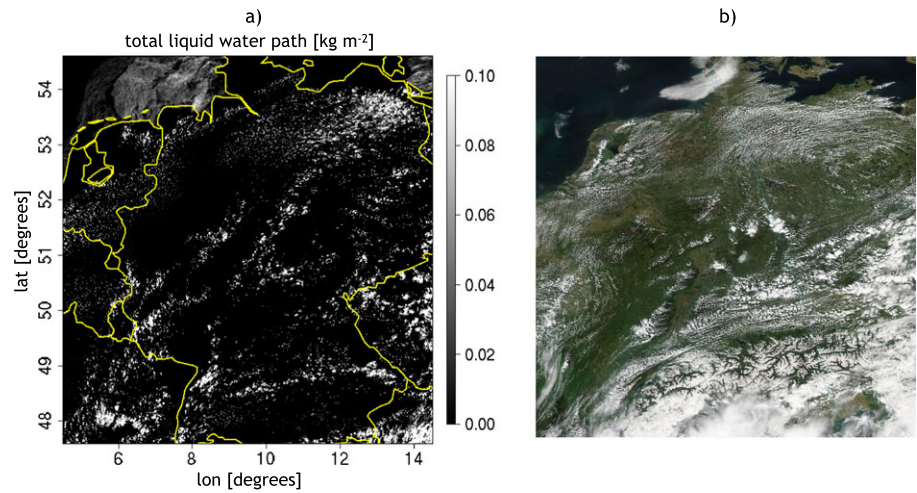
a)
total liquid water path [kg m^{-2}]

b)

Figure 5. A map showing the total liquid water path taken at 12:15 local time of the large eddy simulation at 156-m resolution (a), and a MODIS Aqua image from NASA Worldview (b). MODIS = Moderate Resolution Imaging Spectroradiometer.

values and very low probability of higher mass flux values, and much higher variability compared to the bulk mass flux values (see Figure 7). This idea would, however, need to be tested further for any other application.

3. Results

3.1. A Shallow Convective Day Over Germany

The simulated test case is 5 May 2013, which was a prevalently shallow convective day with very little precipitation. A LES of the same day is used as a reference case to test the three different model configurations made of the deterministic shallow convection parameterization as in Bechtold et al. (2014), the configuration with no convection parameterization and the configuration that includes the stochastic version of shallow convection. All four simulations are initialized at midnight using the Consortium for Small-scale Modeling (COSMO) analysis (Baldauf et al., 2011) and are nudged at the lateral boundaries toward 1-hourly COSMO analysis, exactly as in the study of Heinze et al. (2017). All simulations are run for 24 hr.

The LES is performed using ICON-LES with a horizontal resolution of 156 m as one of the test simulations of the HD(CP)^2 project (Heinze et al., 2017). We compare the map of the liquid water path that results from the LES with a satellite image (Figures 5a and 5b). The cloud field looks realistic with all the relevant features of convective cloudiness reproduced well by the LES: the shallow convective region in the northeast of Germany, more isolated larger convective events in the central regions, the orographic effects on convection in the southeastern regions and scattered convection in the south. Also visible is the snow cover over the Alps, which might make it difficult to visually isolate the clouds on the satellite image. Convective rolls and other
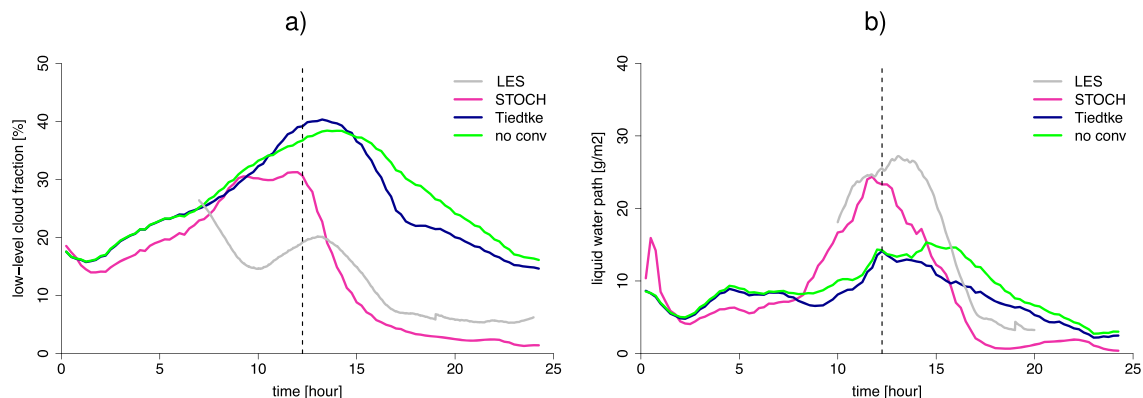
a)

b)

Figure 6. Time series of the (a) low-level (<800 hPa) cloud fraction and (b) liquid water path from the four ICON simulations at 1.2 km resolution for the entire region (48–54°N; 6–14°E). ICON = icosahedral nonhydrostatic model.
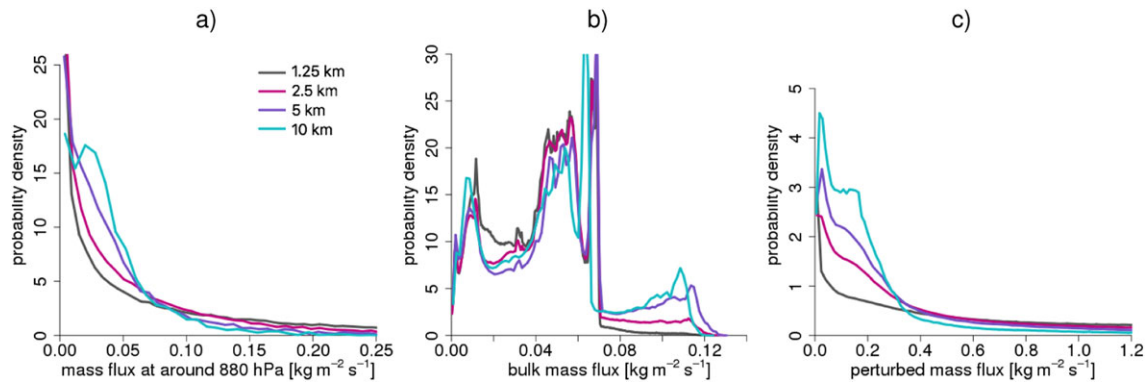
Figure 7. The distribution of the total mass flux M resulting from the (a) coarsened LES, (b) deterministic convection, and (c) stochastic convection. In the case of the stochastic convection, M is the sum over all clouds present at a given time step, while in the case of the deterministic convection, M is the bulk mass flux in a given grid cell. The reference LES distributions (a) are calculated by taking the cloud fraction in each grid cell and multiplying it with the vertical velocity in that cell at the single level near the average cloud base around 880 hPa.

organization patterns that can be identified as cloud lines visible on the satellite image are not so evident in the LES cloud liquid water map. It is possible that a higher grid resolution is necessary to resolve the realistic convective rolls and cloud lines in LES.

The time series of the low-level cloud fraction, defined as the fraction of clouds below 800 hPa, are plotted for all four ICON model configurations (Figure 6a). The reference LES case shows two peaks in cloud fraction early in the morning and around 13 hr local time. The deterministic simulation produces a single peak around 13 hr; however, its magnitude is largely overestimated. The simulation that includes no convection parameterization also shows a single peak with a delay of about 1 hr and with an overestimation of cloud fraction by about 20% in its absolute value. The stochastic simulation does not reproduce the two peaks correctly; however, the magnitude and overall behavior matches the LES simulation more closely than the other two cases.

A single pronounced peak is evident in the time series of the liquid water path averaged over the entire domain in the reference LES simulation (Figure 6b). The liquid water path is underestimated in both deterministic and no-convection case, while the stochastic version matches the LES liquid water path better. The case that includes no subgrid convection shows a delay of a couple of hours in the maximum of the liquid water path time series, while the stochastic case shows a peak in the liquid water path about 1 hr earlier compared to the LES simulation.

3.2. Scale Awareness in the Formulation of Subgrid Convection

The scale-awareness in the formulation of subgrid convection can be assessed by testing how well the scheme reproduces the predicted changes in the shape of $p(M)$ with changing model resolution (section 2.2.1, Figure 2). We use the LES fields coarsened over the grids of four different resolutions (from 1 to 10 km) as a reference for the ICON simulations. As the resolution increases, the LES results suggest a change in the distribution shape toward a long-tailed distribution, where the probability density of small mass flux values gradually increases at the cost of the higher values (Figure 7a). At the same time, due to longer tails, the larger mass flux values become more probable on higher than on coarser resolutions; however, they still count as rare events.

The deterministic closure of the Tiedtke-Bechtold scheme produces distributions of the total mass flux $p(M)$ that have similar shapes on all grid resolutions and show pronounced high peaks at certain values (Figure 7b). This similarity across resolutions is caused by the bulk formulation of the mass flux closure that is not designed to reproduce an increasing variability of the mass flux as the model resolutions increase into the gray zone. The high and irregular peaks are a direct result of the imposed safety limiters for the mass flux values, which remain active in the deterministic version of the scheme. As a result of these two factors, the shapes of $p(M)$ in the deterministic simulations do not resemble the expected shapes estimated from the LES results (Figure 7a).

As described in section 2, the bulk mass flux closure is designed for the coarse grids and is not intended to work in the gray zone. In the gray zone, the bulk closure might produce a too strong convective mass flux in most of the grid columns, which might cause a too strong influence of subgrid convection on the resolved convective dynamics and produce no convective activity in the next time step. In this way, the subgrid convection
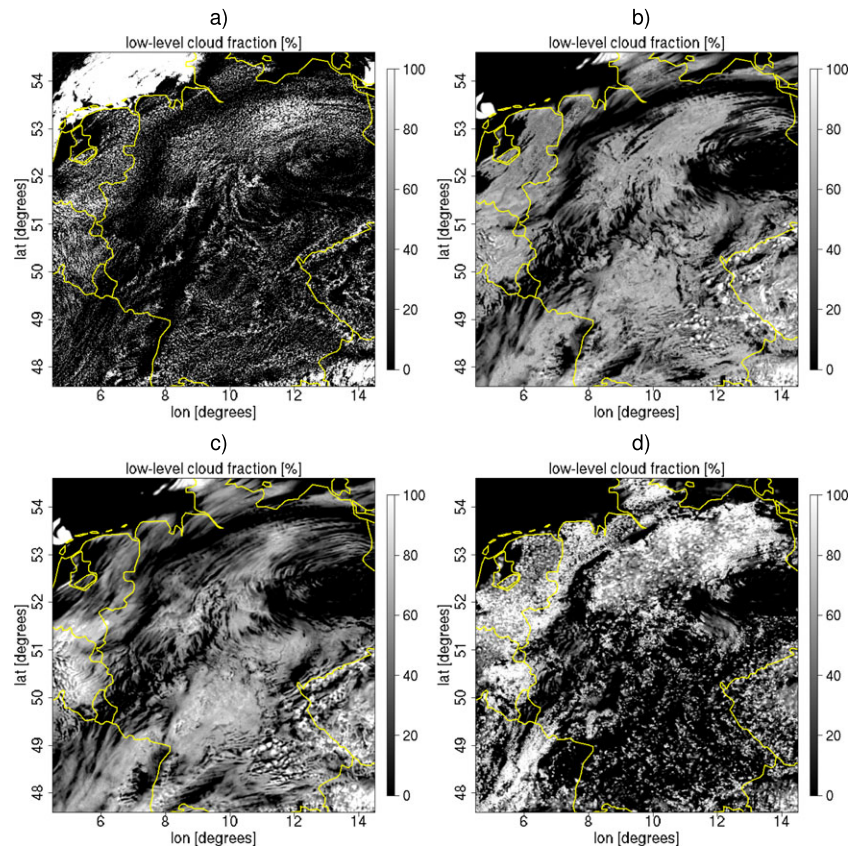
Figure 8. Maps of the low-level cloud fraction for different ICON model configurations taken at 12:15 hr: (a) Large eddy simulation coarsened to 1.2 km, (b) Tiedtke-Bechtold shallow convection, (c) no convection parameterization, and (d) stochastic shallow convection.

becomes a source of artificial noise in the resulting convective flow. Thus, in addition to the flow instabilities caused by too frequent and too high mass flux values, this source of artificial noise is one more reason to impose the mass flux safety limiters in the gray zone. Thus, when such a deterministic scheme is used, the safety limiters inevitably affect the mass flux distribution $p(M)$ in an unfavorable way (Figure 7b).

By correcting the values of the subgrid total mass flux using the newly introduced stochastic sampling, it is possible to remove the mass flux limiters and other restrictions on the convective activity in the convection scheme, as already suggested in section 2.2.5. This allows for the leading role of the stochastic sampling in shaping of the mass flux distributions across different resolutions, which results in a scale-aware $p(M)$ (Figure 7c). The shapes of $p(M)$ are very similar to the shapes of the coarsened mass flux distributions calculated from the LES output, and they follow the same scale-aware behavior. So the stochastic formulation of the mass flux introduces a correct scale awareness into the parameterization of convection.

In the case of the ICON-LES, the total mass flux in each coarsening bin is calculated by taking a single-model level (at around 880 hPa) and by multiplying the cloud fraction at that level with the average vertical velocity in the same coarse box. The difference in the values between the mass flux in LES and the values that result directly from the parameterization of shallow convection at different resolutions comes mostly from the different estimation of the cloud base level in the two cases. The level at which the LES mass flux is calculated is slightly below the cloud base peak of the cloud fraction (see Figures 12).

3.3. Spatial Distribution of Cloudiness

Maps of the low-level cloud fraction as a result of the simulations conducted using the three different ICON model configurations are compared with the reference map resulting from the ICON-LES simulation (Figure 8). The maps are extracted from the single time step at 12:15 hr local time, which is indicated by the vertical dotted line on Figure 6. The deterministic parameterization produces too much cloudiness overall in spatial coverage (Figure 8b), while it does not capture the localized high values of the cloud fraction as expected
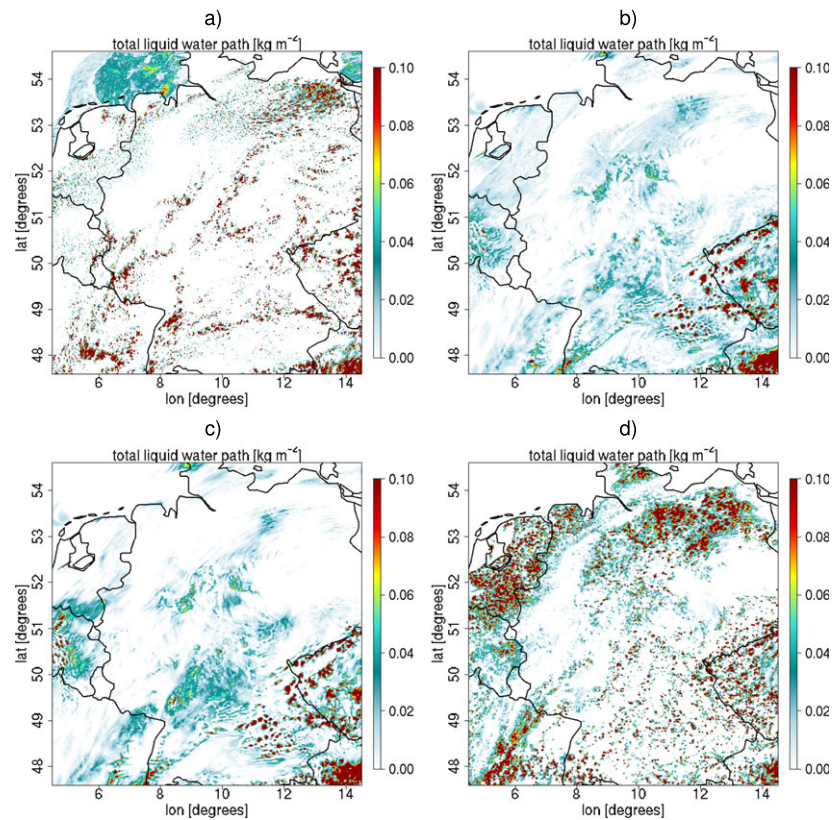
Figure 9. The maps of the cloud liquid water path plotted for the time step at 12:15 hr: (a) Large eddy simulation coarsened to 1.2 km, (b) Tiedtke-Bechtold shallow convection, (c) no convection, (d) stochastic shallow convection.

based on LES (Figure 8a). When the convection parameterization is switched off, the model dynamics take over the entire convective transport which results in overestimation of the average cloud fraction, too wide spatial coverage and too strongly organized convection (Figure 8c). This organization manifests itself by too regular cloudy stripes extending over the shallow convective regions. The deterministic and no-convection cases show a very similar behavior. This indicates that the resolved dynamics are dictating the convective activity and the behavior of the convection scheme, while the subgrid convection has no effect on the regime of the resolved convective flow. The stochastic version of shallow convection introduces more spatial variability in cloud fraction (Figure 8d), which resembles the LES field closer than the other two configurations (Figure 8a). The strong artificial organization patterns are diminished by the stochastic perturbations and the cloud cover field appears more noisy which is closer to the LES result. The stochastic version reduces the midrange values of cloud fraction and its spatial coverage resulting in a significant improvement.

The total liquid water path is largely underestimated in magnitude and in variability in the case of simulations with the deterministic and without any convection scheme, while the spatial coverage is overpredicted, see Figures 9b and 9c. This is a consequence of the underresolved convective circulations that are weaker than expected at these scales and cover spatially too broad regions (see section 3.5). In the case of the stochastic convection, the magnitude and spatial variability of the liquid water path is better predicted than in the other two cases (Figure 9d). However, in the northern regions, shallow convection is largely overestimated. In the northern regions of the domain, shallow convection is too active at this time step and it peaks sooner than the convection produced by LES and the other two configurations of ICON. When judging the results presented on these plots, we also have to take into account that at the time for which the maps are plotted (12:15 hr), the four cases were at different stages in the diurnal cycle.

To examine the spatial distribution of the low-level cloud fraction, total cloud cover and total liquid water path in a more quantitative way, the probability densities are calculated by collecting the samples every hour from 10 to 15 hr of the simulation in the entire modeling domain (Figure 10). The fields of cloud properties that resulted from LES were first coarsened to reflect the expected outcome at a given resolution used in the
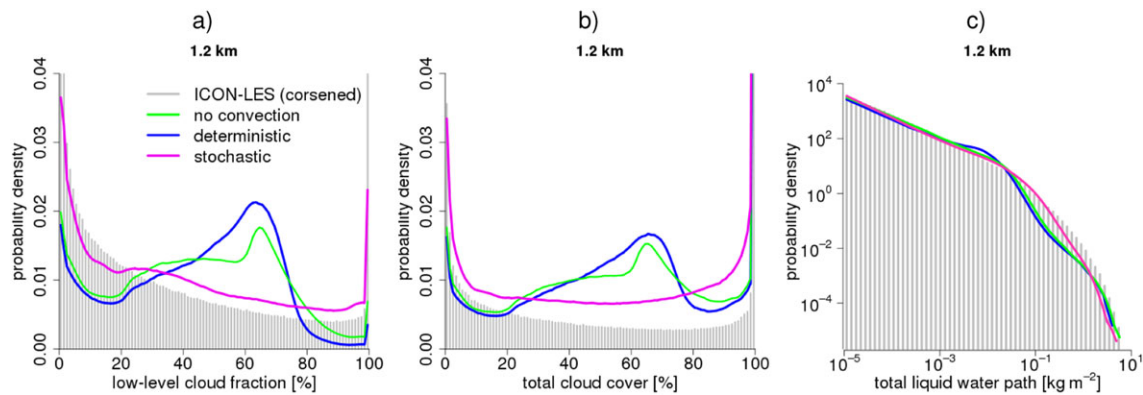
Figure 10. Distribution plots of the low-level cloud fraction (a), total cloud cover (b), and total liquid water path on a log-log plot (c), all at the resolution of 1.2 km. Samples are collected from snapshots taken each hour from 10- to 15-hr local time and are combined in the distribution plots. ICON = icosahedral nonhydrostatic model; LES = large eddy simulation.

simulations with parameterized shallow convection, then such coarsened values of cloud fraction are used to calculate the probability density distribution (gray colored bars). The reference LES simulation produces the distributions of the low-level cloud fraction and the total cloud cover (Figures 10a and 10b) that show a high probability of occurrence of low and very high cloud fractions and lower probability of the midrange cloud fractions. The distribution of the total liquid water path (Figure 10c) that results from the reference simulation has a long-tailed shape.

Taking the LES distributions as a reference, the model configuration that includes the stochastic convection produces the most correct cloud fraction and total cloud cover distributions of all three configurations (Figures 10a and 10b). The shape of the distribution in the case of stochastic convection follows the shape imposed by the mass flux sampling and resembles the shape of $p(M)$ (Figure 7c). The configurations that include deterministic convection and no convection parameterization overestimate the midrange values of the cloud fraction, as the distributions have pronounced peaks at these values. These shapes of the distributions are consistent with the distribution of the cloud fraction in maps presented in Figure 8, showing vast regions covered with the midrange values of cloud fraction in the cases that include no convection and deterministic convection, while more extremes, less midrange values, and less spatial coverage are present in the case of stochastic convection.

In a similar way to the cloud fraction distribution, the distribution of the total liquid water path is improved when using the stochastic convection (Figure 10c). This improvement is evident across a wide range of the liquid water path values that constitute the distribution body, except for the highest values in the distribution tail. These distributions explain the spatial maps of the total liquid water path (Figures 9b and 9c), as the cases of deterministic and no convection parameterization show the peaks in the liquid water path at the midrange values. These high peaks at the midrange values of the liquid water path are not supported by LES.

The improved spatial variability of cloudiness in the simulations that employ the stochastic parameterization of convection (Figure 10) comes from the effects that subgrid convection has on the resolved convective dynamics when the mass flux limiters are inactive, while the stochastic sampling of the mass flux distribution further corrects the shape of the distributions. The spatial distribution of cloudiness is corrected by the stochastic sampling indirectly by changing the mass flux values at the cloud base and not by introducing a stochastic triggering of convection. The resolved convective dynamics is influenced by the stochastic perturbations, which then affects the triggering of convection in the subsequent time steps and produces different spatial distribution compared to the deterministic version of the scheme. We will show more about the effects of parameterization on the resolved dynamics in section 3.5.

One has to keep in mind that the purpose of the present study is to evaluate the new formulation without the additional tuning, keeping in mind that the new stochastic scheme might not be compatible with all components of the parameterization of subgrid physical processes. Further cases and different synoptic situations need to be considered, before revisiting and recalibrating the physics package for optimal weather forecasts.
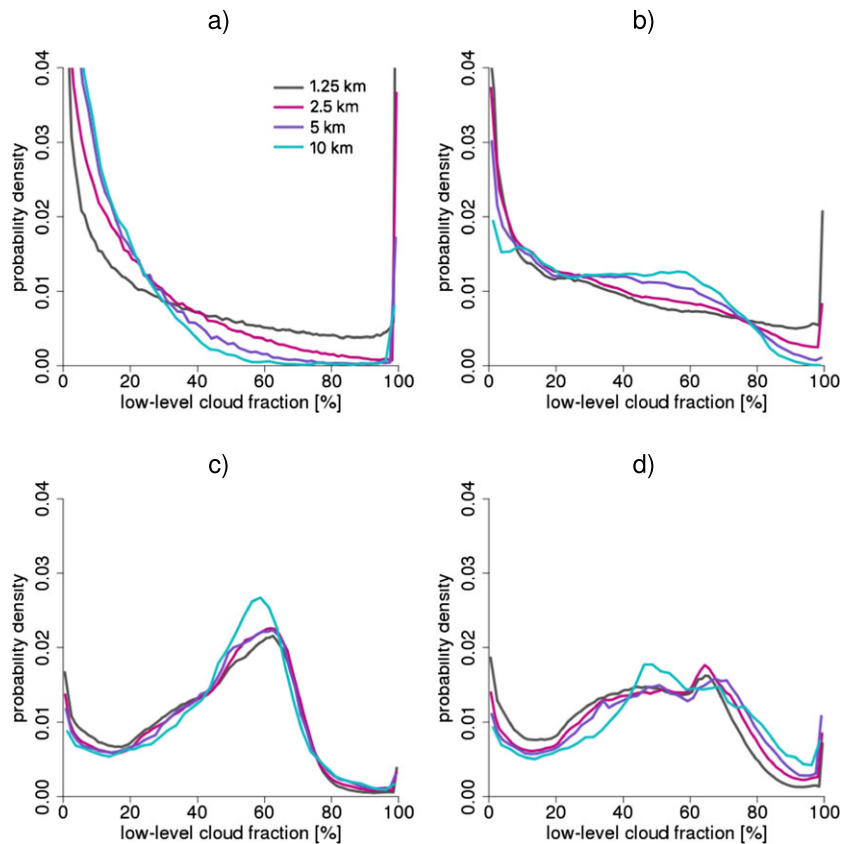
Figure 11. The distribution of the low-level cloud fraction, defined as the fraction of clouds below 800 hPa, resulting from the (a) coarsened large eddy simulation, (b) stochastic convection, (c) deterministic convection, and (d) no subgrid convection.

3.4. Scale Awareness in the Simulation Results

Based on the results of the LES, we estimate how the distribution of the low-level cloud fraction should change with model resolution in ICON (Figure 11a). As the resolution decreases there are gradually less grid columns with the high values of cloud fraction, but at the same time more columns with the small values of cloud fraction. So the scale awareness of the cloud fraction distributions manifest itself in the change of the slope of the distribution from less to more steep, while the peak at the 100% cloud fraction decreases. This behavior closely follows the change in the mass flux distributions with resolution (Figure 7a).

At 10-km horizontal resolution the stochastic version of shallow convection struggles to reproduce the shape of the distribution for low-level cloud fraction, as biases of the bulk convection dominate (cf. Figures 11b and 11c). At higher resolutions the stochastic scheme makes the distribution of low level clouds converge to a comparable shape to the LES distribution. The stochastic convection eventually converges toward a spectral distribution of clouds at the high model resolutions, which could be a reason for a better agreement with LES as the resolution increases. In contrast to the stochastic parameterization, the deterministic model setup shows no scale awareness in the distribution of cloud fraction (Figure 11c).

Subgrid formulation of the convective mass flux is not the only factor that influences the scale awareness of the simulation results. The resolved dynamics is equally, if not even more, important to achieve scale awareness as it affects the change in the distributions with model resolution in the opposite way from what is suggested based on LES (Figure 11d). The bell shape of the distributions in Figure 11d is similar across all resolutions, which does not resemble the distributions that result from coarsening of the LES output (Figure 11a). In addition, with coarsening of the resolution, the resolved dynamics produces more high cloud fraction columns and less columns with low cloud fraction which is the opposite of the expected behavior. The subgrid formulation of the stochastic sampling can only correct this behavior of the underresolved dynamics to a limited extent and mostly at the 1- to 2-km resolutions (Figure 11b).
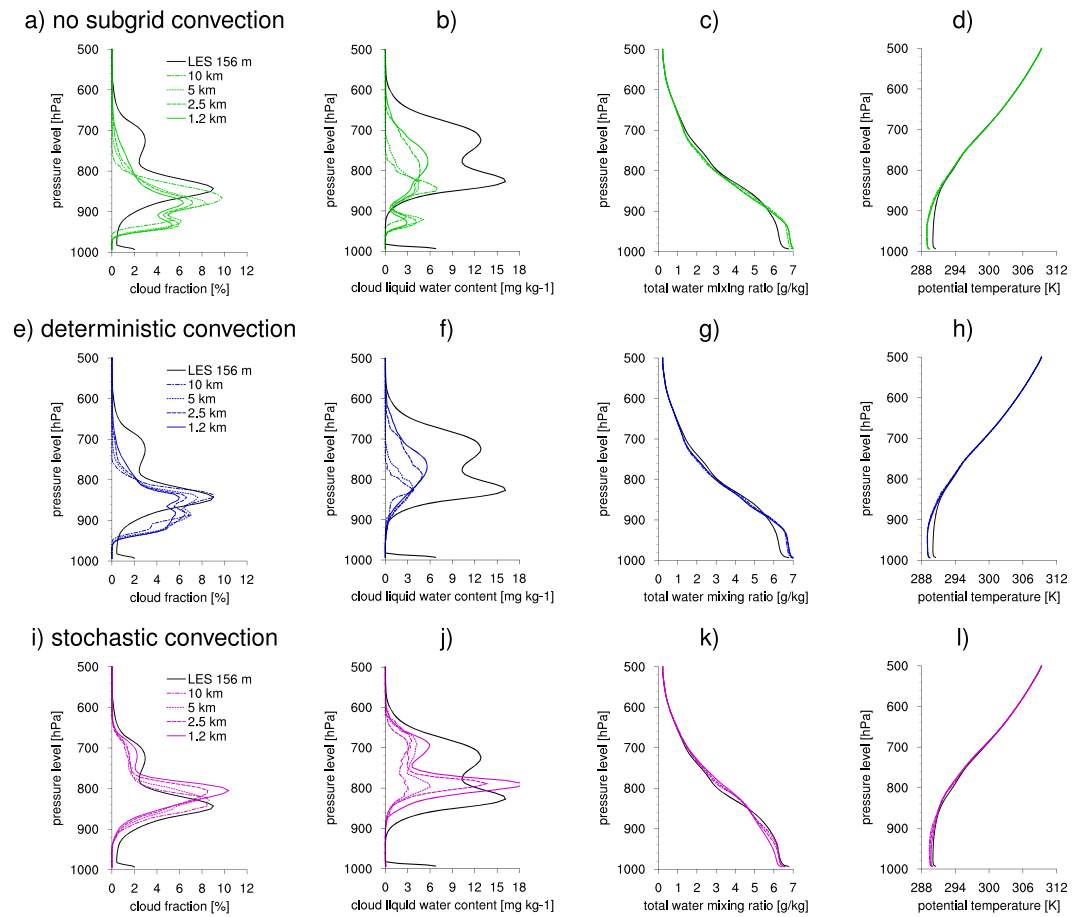
Figure 12. Vertical profiles plotted from the time step at 12:15 hr for the entire region excluding the domain edges (48–54°N; 6–14°E). In the first line (a–d, green), the vertical profiles that result from the simulations where the convection parameterization was not active are shown. The second line represents the vertical profiles when a default deterministic parameterization is used (e–h, blue), and the third line when the stochastic parameterization is used (i–l, magenta). The reference LES profiles are drawn in black lines. LES = large eddy simulation.

By introducing scale awareness in the distribution of cloud properties, the mean state and the vertical structure of the atmosphere should not be affected and should not change with the model resolution. We show the vertical profiles of cloud fraction, cloud liquid water, total water mixing ratio, and potential temperature for all four ICON configurations at resolutions in the range from 1 to 10 km (Figure 12). Cloud fraction and liquid water content show some difference across resolutions in all cases (Figure 12a,b,e,f,i,j), while the vertical profiles of total water mixing ratio and potential temperature stay similar across different resolutions (Figures 12c, 12d, 12g, 12h, 12k, and 12l).

In the cases shown on Figures 12a and 12b, where subgrid convection is not parameterized, the profiles are not similar to the LES results because convection is not properly resolved at these resolutions. The convection is too weak in these two cases and it shows a different timing of the onset and a delayed peak in the cloudiness over the diurnal cycle (Figure 6). The vertical cloud profiles in the deterministic case (Figures 12e and 12f) are very similar to the case without subgrid shallow convection (Figures 12a and 12b), which indicates that the convection parameterization is not affecting the resolved dynamics to a great extent. In both configurations, deterministic and no subgrid convection, the cloud base height is too low and the cloud liquid water content is underestimated.

The stochastic version of the convection parameterization improves the profiles of cloud fraction and liquid water content (Figures 12i and 12j). The cloud base height is slightly higher than in LES, but the structure of the cloud layer with a peak near the cloud base and near the top of the layer is well reproduced. This is achieved with no tuning of the parameters in the stochastic scheme nor in the underlying convection scheme.
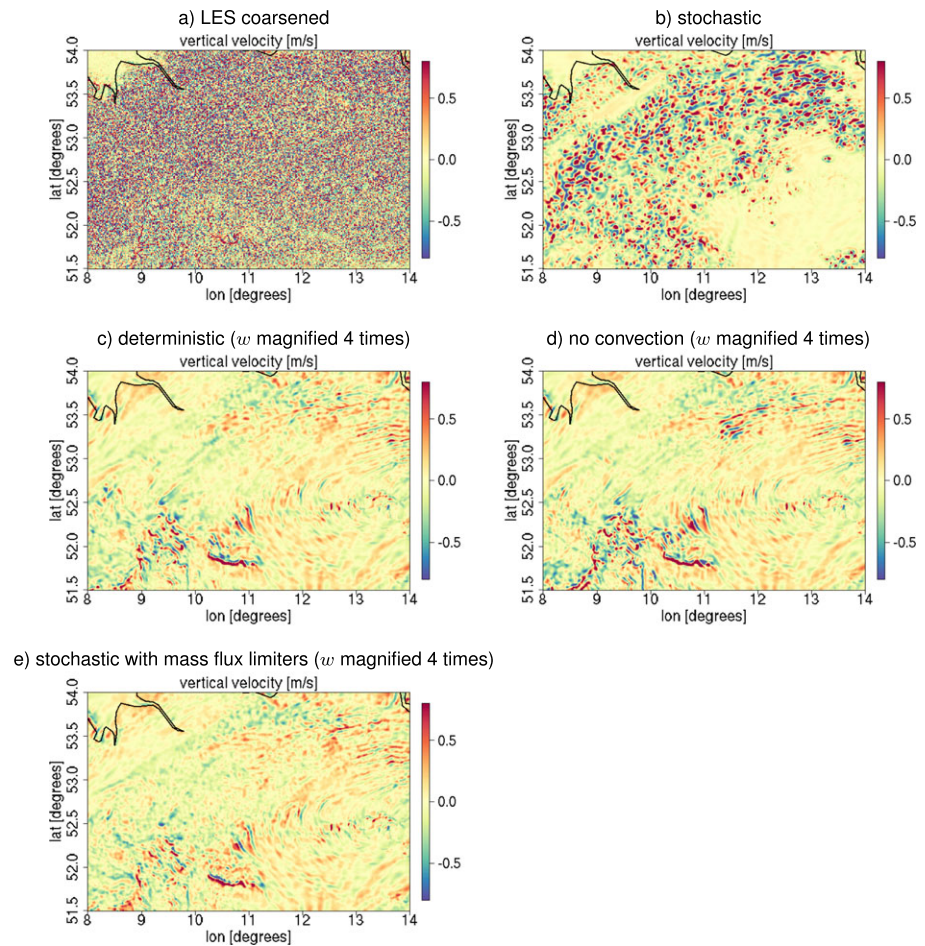
Figure 13. Horizontal cross sections of vertical velocity near the cloud base for different icosahedral nonhydrostatic model configurations at 1.2-km resolution in the northeastern Germany: (a) LES coarsened to 1.2 km, (b) stochastic version of the Tiedtke-Bechtold shallow convection, (c) default version of the Tiedtke-Bechtold shallow convection, (d) no convection parameterization, and (e) stochastic version including the mass flux limiters. LES = large eddy simulation.

This significant improvement results from subsampling of the mass flux distribution $p(M)$, which introduces a correct variability of the convective activity in the modeling domain, and by an unbounded interaction of subgrid convection with the resolved dynamics. In the case of the stochastic configuration, the subgrid convection changes the strength and the regime of the resolved flow, which results in the vertical profiles that match the LES results better than the other two configurations. The bulk representation of convection converges with the stochastic scheme toward a spectral representation of convection for the higher resolutions. We study the interaction between dynamics and stochastic parameterization in more detail in section 3.5.

The vertical profiles of potential temperature and total moisture are well predicted above the boundary layer in all cases. Within the boundary layer the biases are strongly reduced in the simulation with the stochastic shallow convection parameterization relative to the LES from the other cases (Figures 12k and 12l). This improvement originates from corrected values of the cloud base mass flux compared to the deterministic version of the scheme partly because of removal of the limiters and partly due to the correction by stochastic sampling. Only in the stochastic version of the parameterization, the limiters can be removed to get the correct mean state. In addition, the stochastic perturbations produce the correct mean state without additional tuning. A small change with resolution is visible in the subcloud layer in the case of Figure 12k.

3.5. Resolved Convective Circulations
In the convective gray zone, emerging convective circulations have properties that are highly dependent on the gird resolution (Ching et al., 2014; Zhou et al., 2014). As a result, these convective circulations are weaker than expected relative to the coarsened LES output. This is demonstrated by the maps of the vertical
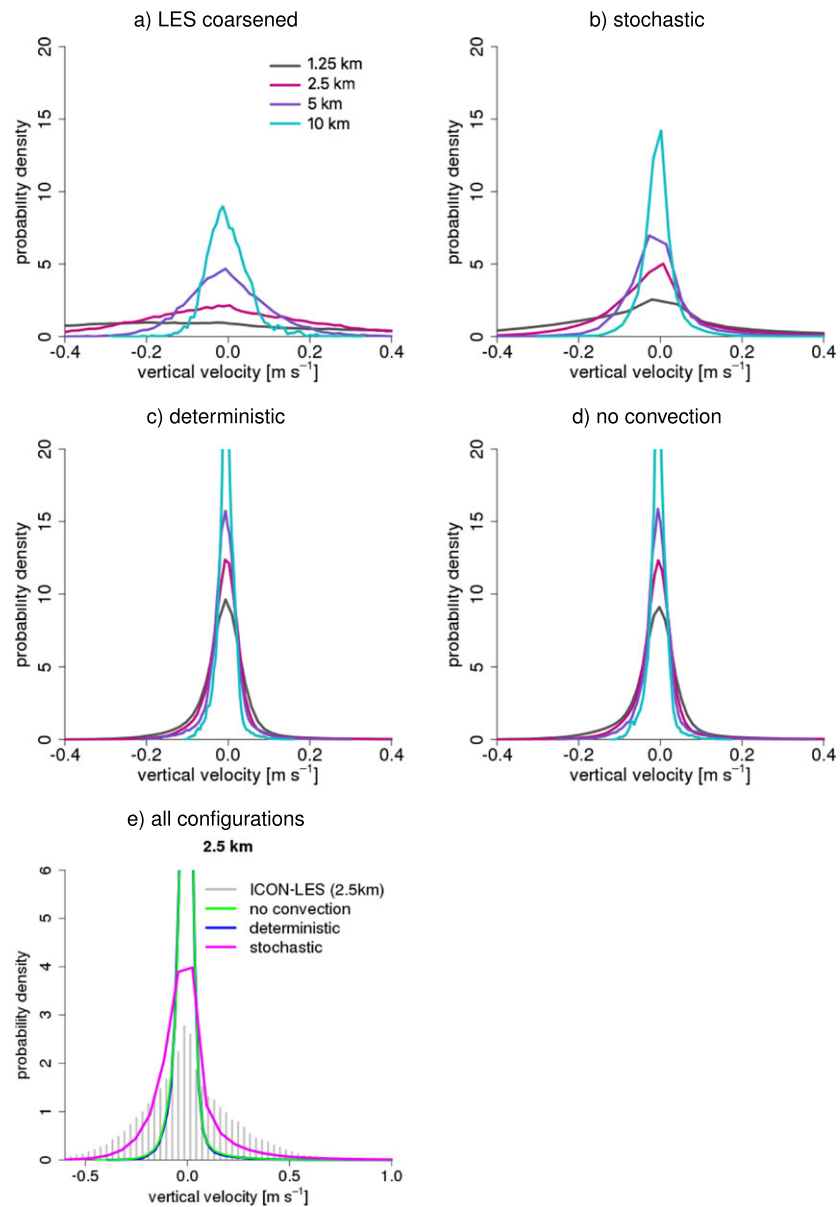
Figure 14. Histograms of the vertical velocity at different resolutions for all four Icosahedral Nonhydrostatic model configurations: (a) LES coarsened to mimic the resolutions from 1 to 10 km, (b) stochastic version of the Tiedtke-Bechtold shallow convection, (c) default version of the Tiedtke-Bechtold shallow convection, (d) no convection parameterization, and (e) all configurations at 2.5 km resolution. LES = large eddy simulation; ICON = icosahedral nonhydrostatic model.

velocity (Figure 13) and the probability distributions of vertical velocity plotted for all four ICON configurations (Figure 14; see also Sakradzija et al., 2016). In addition, strongly organized convective line patterns emerge in these simulations; however, such organized structures are not realistic and have a too wide horizontal dimensions of updraft and downdraft regions (Figure 13d). Such strong organization is not a property of natural convection that would correspond to the model resolution at hand and is not comparable to the LES results (Figure 13a). The coarsened LES results suggest no visible organized patterns at the selected resolution, and the vertical velocity appears randomly distributed.

The deterministic version of the ICON convection produces very similar convective patterns to the simulation that includes no convection parameterization (Figure 13c). The deterministic convection parameterization has almost no power to influence the convective regime of the resolved flow and emerging organized patterns. The reason for this are the mass flux limiters discussed in section 3.3. Thus, in this case the resolved convective
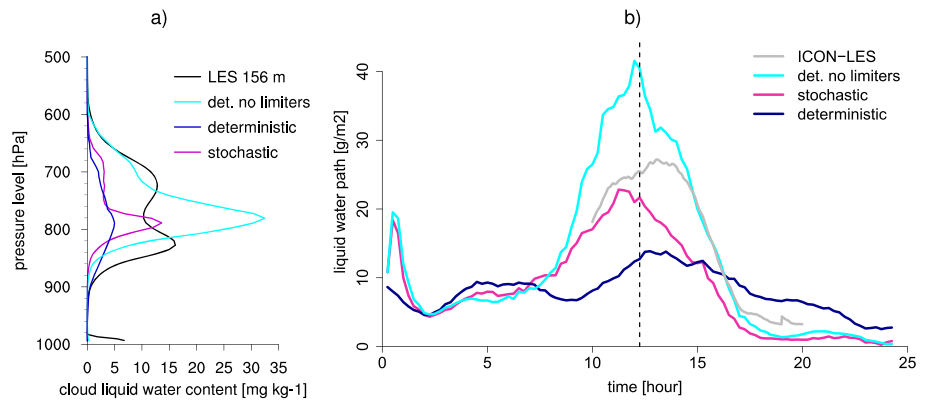
Figure 15. (a) Vertical profiles of the total cloud liquid water content in the case of deterministic convection scheme that includes the mass flux limiters (blue), stochastic (magenta), and deterministic convection (cyan) both without the mass flux limiters and before tuning; (b) time series of the liquid water path showing the three simulations against LES. Both plots are corresponding to the simulations at 2.5-km resolution. LES = large eddy simulation; ICON = icosahedral nonhydrostatic model.

dynamics fully controls the subgrid parameterization. This is in no way desirable, because these convective circulations are not realistic, and the incorrect forcing of the parameterization can only produce an incorrect tendency back to update the resolved flow (see, e.g., Lander & Hoskins, 1997).

The stochastic scheme itself has a very limited effect on the underresolved circulations before the mass flux limiters are disabled in the convection routines (Figure 13e). The convective patterns in this case do not differ significantly from the patterns observed in the simulation using the deterministic configuration. When the mass flux limiters and the limiters of the shallow convection activity are disabled, the strength and organization regime of the resolved convection changes (Figure 13b) as predicted in the study of Sakradzija et al. (2016). The convective circulations increase in strength up to approximately a factor of 4, while the updraft and downdraft regions are more randomly distributed, which resembles the coarsened LES field of vertical velocity closer than the other two configurations.

For a more quantitative comparison of the strength of the convective circulations we plot the histograms of vertical velocity for all four model resolutions and for all four ICON model configurations (Figure 14). As the model resolution coarsens, the variance of the vertical velocity decreases and the histograms become narrower in all model configurations (Figures 14a–14d). The stochastic simulations show the most similar histograms to the LES results on all resolutions (b), while the deterministic (c) and no-convection case (d) show much narrower histograms that do not reflect the correct behavior based on LES and that largely underestimate the variance of vertical velocity. A closer look at the histograms for 2.5-km resolution (e) shows that the two latter cases have almost identical w histograms, while the stochastic case is approaching LES result even

Table 4
List of the Parameter Sensitivity Experiments

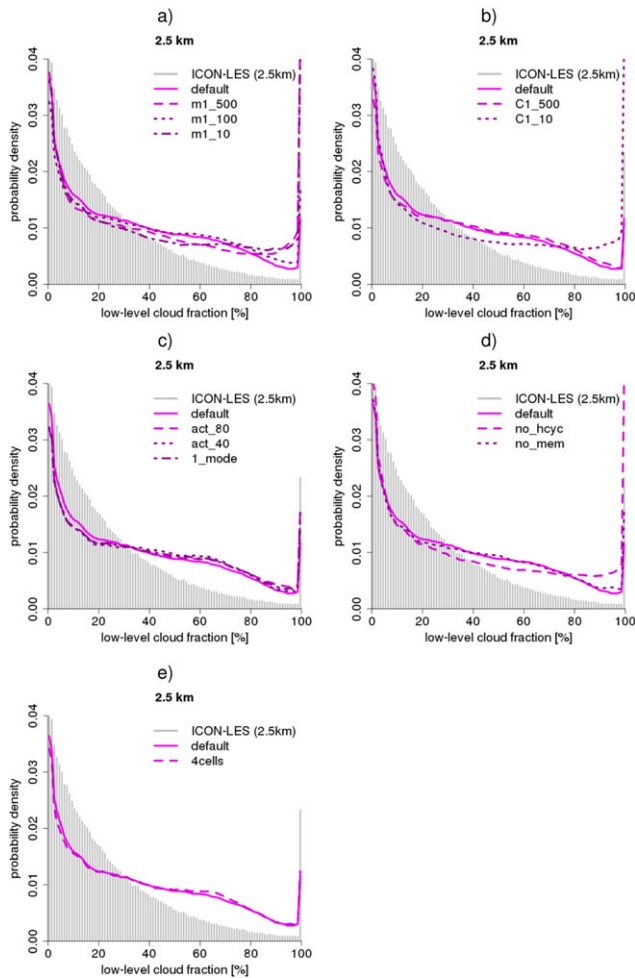| Parameter	Value	Unit	Test flag
$\langle m_1 \rangle$	500,000	kg/s	m1_500
$\langle m_1 \rangle$	100,000	kg/s	m1_100
$\langle m_1 \rangle$	10,000	kg/s	m1_10
C_1	500,000	kg/s	C1_500
C_1	10,000	kg/s	C1_10
f_{act}	80	%	act_80
f_{act}	40	%	act_40
Single mode	100	%	1_mode
No heat cycle constraint	equation (10)	–	no_hcyc
No lifecycles and memory	-	–	no_mem
Averaging	over 4 cells	-	4cells

Figure 16. (a–e) Sensitivity of the distribution of the low-level cloud fraction on the parameters in the stochastic convection routine. The plots correspond to the experiments listed in the Table 4. ICON = icosahedral nonhydrostatic model; LES = large eddy simulation.

though it is still lacking some variance. In contrast to the results shown here, the w variance was over-predicted by the stochastic version of the EDMF scheme in the study of Sakradzija et al. (2016). The reason for this was most likely a direct interaction of convection with the turbulence parameterization in the boundary layer, which is inherent in the EDMF parameterization (Siebesma et al., 2007).

Based on these results, the question arises as to what is the behavior of the deterministic convection parameterization when no tuning is done and when no mass flux limiters are used. In that case we also observe the interaction with the resolved dynamics that invigorates the resolved convective flow (not shown here). However, such interaction is prone to the artificial noise that cannot be constrained in any physical way, as discussed in section 3.2. In this case, the effect that the deterministic parameterization has on the resolved dynamics can be controlled only by tuning and by imposing the mass flux limiters. For example, if the limiters of convective activity are not employed in a deterministic configuration, the overly invigorated resolved convection produces too much cloud liquid water, an incorrect cloud layer structure (Figure 15a), and an almost doubled maximum liquid water path over the diurnal cycle compared to the reference LES case (Figure 15b).

3.6. Tests of Parameter Sensitivity

In this section, we test the sensitivity of the simulated cloud fields on the choices in the parameters and setup of the stochastic scheme. We avoid tuning on a single case and for a narrow target, but document sensitivities for future optimization of model performances using the here presented parameterization. The experiments in which these tests are undertaken are listed in Table 4. We focus on the differences in the low-level cloud fraction distribution plots that arise because of the differences in parameters. All tests are performed at 2.5-km resolution.

The most sensitive parameters are the average mass flux of passive clouds $\langle m_1 \rangle$ and the minimum possible average mass flux of active clouds C_1. C_1 is the fitting parameter of equation (10) estimated in the LES study of Sakradzija and Hohenegger (2017). The default values of these parameters are given in Table 3. An unrealistically wide range of values for these two parameters is tested (Table 4). In both cases, changing the parameter value to a very low (m1_10, C1_10) or to a very high value (m1_500, C1_500) produces lower probability of occurrence of low and midvalues of the low-level cloud fraction, while the probability of high values of the cloud fraction gets even more overestimated (Figures 16a and 16b). Based on these tests, the default values for $\langle m_1 \rangle$ and C_1 estimated using LES are the best choice for these two parameters for the simulated low-level cloud fraction. On the other hand, the parameters $\langle m_1 \rangle$ and C_1 affect the histograms of the vertical velocity (see Figure 17a for the sensitivity to C_1) and could be tuned to produce more w variance and stronger resolved convective flows.

The fraction of partitioning into the passive and active cloud modes is the least sensitive parameter of the stochastic scheme that was tested here. There are no apparent changes in the cloud fraction distributions if the active cloud mode fraction is increased gradually from 40 to 80% (Figure 16c). Thus, our choice and recommendation is to keep the active cloud fraction at its default value of 60% (Table 3). Selecting a unimodal function to describe the cloud mass flux distribution in the stochastic sampling made no difference to the cloud fraction distribution (Figure 16c) compared to the default configuration.

As a next test, the two alternative configurations of the stochastic scheme are used: a configuration with no memory over the cloud life cycles (no_mem), and the configuration without the constraint of the convective heat cycle, equation (10) (no_hcyc). The case no_mem is set up by changing the parameters β and k from 0.8 to 1, $\beta = 1$, $k = 1$, and by using the average mass flux over the cloud life instead of a life cycle function (referenced in section 2.2.1). In the no_hcyc case the formulation of the stochastic scheme from
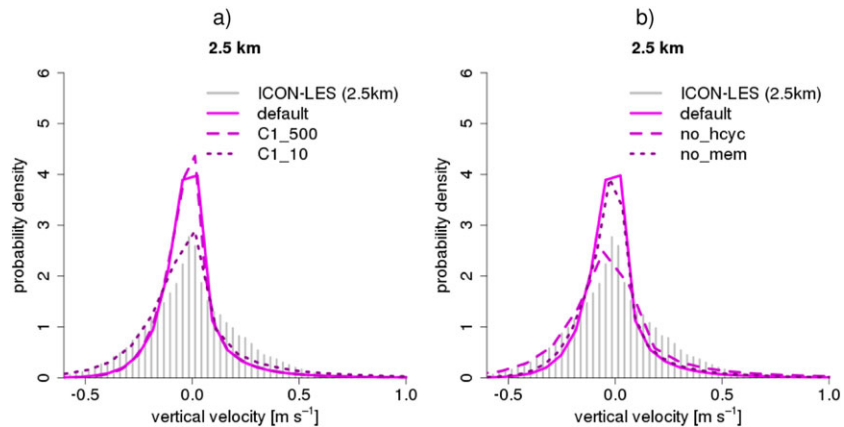
Figure 17. Sensitivity of the histograms of the vertical velocity on the choice of the value of the (a) parameter C^1 and (b) the configuration of the stochastic scheme. ICON = icosahedral nonhydrostatic model; LES = large eddy simulation.

Sakradzija et al. (2015) is used. The lack of memory in the no_mem case causes more large values of cloud fraction (90–100%) compared to the default case. The effect of excluding the heat cycle constraint is a flatter distribution shape and an even larger overestimation of the high cloud fractions. Neither of the two cases are an improvement compared to the default case (Figure 16d) in reproducing the distribution of the low-level cloud fraction. However, the configuration no_hcyc does make a difference for the vertical velocity variance (Figure 17b) and could be used as a tuning parameter to affect the strength of the resolved convective circulations.

The choice for the averaging scale of the input for the first call of the convection scheme over neighboring 3 (4 in total) or 12 cells (13 in total) does not make a difference for the resulting low-level cloud fraction distribution plots (Figure 16e) at this resolution.

In general, all the tests conducted here gave a low sensitivity to the stochastic scheme parameters and its configuration choice. The shape of the cloud fraction distribution remains very similar to the shape of the distribution in the default configuration, except in those cases that involved unrealistic parameter values, such as in the cases m1_500, m1_10, and C1_500. The parameters m1 and C1 seem to be the only tunable parameters in the stochastic scheme that could be used later for fine tuning of the model. This is fully physically justified, because those two parameters determine the average mass flux per cloud $\langle m \rangle$, which is known to be the most relevant parameter to set the shape of the mass flux distribution of individual clouds (Sakradzija & Hohenegger, 2017). The resolved convective circulations can be invigorated further by tuning $\langle m_1 \rangle$ or C_1 and by reconfiguring the stochastic scheme to the no_hcyc case.

4. Summary and Conclusions

In this paper we introduced the stochastic parameterization of Sakradzija et al. (2015) in the ICON model and described its coupling to the Tiedtke-Bechtold parameterization of shallow convection (Bechtold et al., 2014). For the first time, the stochastic parameterization is tested in a model configuration that includes the full subgrid physics package and applied in a realistic case to a single shallow convective day in Germany and surrounding regions. The formulation of the stochastic sampling is fully constrained by the two physical principles: first, the moist static energy convergence (Bechtold et al., 2014) and second, the definition of the moist heat cycle in the cloudy boundary layer (Sakradzija & Hohenegger, 2017). All these points are novelties compared to the previous version of the stochastic parameterization presented in Sakradzija et al. (2016), which was tested in an idealized setup in tropical oceanic conditions using only a boundary layer and shallow cloud parameterization.

The tests include three ICON configurations that differ only in the representation of shallow convection, and the large eddy model (ICON-LES) as a reference. These configurations include the deterministic Tiedtke-Bechtold parameterization, the stochastic version of the same parameterization and a case where the subgrid convection is not active. All configurations are set up for the same specification of the case study and are initialized and forced using the same conditions. The case study covers a single, predominantly shallow

convective day over Germany. The tests were performed using the ICON model at four different horizontal grid resolutions from 1 to 10 km.

In the setup of the model and in performing the tests, we focused on the three aspects that are important for modeling of convection in the gray zone. First, the subgrid shallow convection is formulated to take into account an increasing variability of the cloud base mass flux as the model resolution is increasing. As a second aspect, the effects of this new formulation on the resolved model dynamics in the gray zone are studied, with an emphasis on the strength and regimes of the resolved circulations. And third, the outcome of the choices in the coupling between convection and dynamics are tested. We find that the first two of these aspects are equally important for a correct representation of convection at gray zone scales. The stochastic sampling of the cloud base mass flux alone has no power to correct the overall model behavior unless it is allowed to alter the regime and strength of the resolved circulations. The third aspect of the technical choices in coupling between the new stochastic version of convection and the model dynamics did not show a big impact in this test case.

The unlimited interaction between the stochastic subgrid convection and the resolved convective circulations is achieved by eliminating the artificially imposed safety limiters of the mass flux values in the convection scheme. This can, however, be done only if the stochastic sampling of the cloud base mass flux is included in place of the bulk mass flux closure. In that case, the stochastic version of convection largely improves the spatial distribution of low-level cloud fraction, total cloud cover and liquid water path at the kilometer-scale resolutions. The more active interaction between subgrid and resolved scales also improves the time evolution of the cloud fraction and liquid water path in the case of the stochastic parameterization compared to the other two configurations.

The local perturbations of the subgrid mass flux also help to reproduce the correct large-scale thermodynamic state. This was shown by the average structure of the cloud layer and the vertical profiles of temperature and moisture, which are the most similar to the LES results in the case of the stochastic convection. In the same way as above, the stochastic scheme can not by itself improve the vertical structure of the cloud layer, as it only adds the fluctuations around the mean state in some larger region around the grid column. The mean thermodynamic and cloud layer structure result from the underlying Tiedtke-Bechtold parameterization and the ability to remove the artificial limiters in the convective activity and mass flux once the stochastic perturbations are included.

Another benefit of employing the stochastic sampling and removing the limiters in the parameterization of convection is the ability of the subgrid parameterization to alter the regime and strength of the resolved convective circulations. The artificial organization patterns are removed and replaced by more random convective structures that are closer to the expected noisy convective field produced by coarsening of the vertical velocity in the LES results. The variance of the vertical velocity is improved by the stochastic version of convection compared to the other two ICON configurations, and there is a possibility of further tuning of the stochastic scheme to achieve a better agreement with LES.

In contrast to the ability of the stochastic convection to control the resolved flow regime, the deterministic configuration is fully controlled and lead by the model dynamics and have no ability to change the resolved convective flow. The case configured to include the deterministic convection produces very similar results in the spatial variability of cloudiness, time evolution, and the resolved circulations and their organization patterns to the case that includes no convection parameterization. As a result of imposed limitations on convective activity, the deterministic configuration of convection does not correct the overall results of the simulation and does not provide a significant improvement over the case where convection is not parameterized at all.

By formulation, the stochastic parameterization is scale aware, as the shape of the distribution of the total subgrid mass flux follows the expected changes in the distribution shape based on the LES. However, in the resulting fields of clouds in the simulations that employ the stochastic scheme, the scale awareness is limited. This limitation stems in the first order from the scale dependence of the resolved convective flow, which is demonstrated in the case that includes no parameterization of convection. This case shows changes in the distribution shapes with resolution in the opposite direction from what is expected based on LES. Such behavior across resolutions cannot be fully corrected solely by including the stochastic parameterization of shallow clouds. In addition to the parts of the convection parameterization that were not developed as scale aware in

the first place, other subgrid processes also affect the resolved convective dynamics but were not addressed in the present study. Those processes include the entrainment formulation in the convection parameterization, boundary layer turbulence and microphysics. On the other side, the deterministic configurations of ICON shows no scale-awareness as the distributions of cloud fraction remain very similar across different resolutions and do not resemble the shape suggested by the LES results (Figure 11).

In the evaluation of the new parameterization, one has to keep in mind that the Tiedtke-Bechtold parameterization is a parameterization used operationally at ECMWF and DWD for a long time, and its performance is thoroughly tested and the models are highly optimized. With any changes in the convection parameterization, like introducing the stochastic elements, the whole process chain of the model has to be revisited, which was not done in this study. We did not attempt to tune the model in the new stochastic configuration, because we aimed to show the benefits of adding stochastic fluctuations in the convective mass flux before tuning and also because we did not want to optimize the scheme based on a single case. Furthermore, different effects of the stochastic perturbations might arise when the stochastic scheme is coupled to another convection parameterization.

Taking all the presented results into account, this work demonstrated that by applying the closure at scales where it is valid and by accounting for the fluctuations of subgrid convective states, the modeled convection can be improved to a great extent in the gray zone. A prerequisite for such an improvement is to allow the subgrid convection and stochastic fluctuations to alter the resolved flow dynamics. If so, the benefits can be seen already before any tuning is attempted for any specific resolution in the tested ICON configuration.

References

Ahrens, J. H., & Dieter, U. (1982). Computer generation of Poisson deviates from modified normal distributions. *ACM Transactions on Mathematical Software*, *8*(2), 163–179. https://doi.org/10.1145/355993.355997

Arakawa, A. (2004). The cumulus parameterization problem: Past, present, and future. *Journal of Climate*, *17*(13), 2493–2525.

Baldauf, M., Seifert, A., Förstner, J., Majewski, D., Raschendorfer, M., & Reinhardt, T. (2011). Operational convective-scale numerical weather prediction with the COSMO model: Description and sensitivities. *Monthly Weather Review*, *139*(12), 3887–3905.

Bechtold, P., Semane, N., Lopez, P., Chaboureau, J.-P., Beljaars, A., & Bormann, N. (2014). Representing equilibrium and nonequilibrium convection in large-scale models. *Journal of the Atmospheric Sciences*, *71*(2), 734–753. https://doi.org/10.1175/JAS-D-13-0163.1

Berner, J., Shutts, G., Leutbecher, M., & Palmer, T. (2009). A spectral stochastic kinetic energy backscatter scheme and its impact on flow-dependent predictability in the ECMWF ensemble prediction system. *Journal of the Atmospheric Sciences*, *66*(3), 603–626.

Ching, J., Rotunno, R., LeMone, M., Martilli, A., Kosovic, B., Jimenez, P. A., & Dudhia, J. (2014). Convectively induced secondary circulations in fine-grid mesoscale numerical weather prediction models. *Monthly Weather Review*, *142*, 3284–3302.

Craig, G. C., & Cohen, B. G. (2006). Fluctuations in an equilibrium convective ensemble, Part I: Theoretical formulation. *Journal of the Atmospheric Sciences*, *63*, 1996–2004.

Dipankar, A., Stevens, B., Heinze, R., Moseley, C., Zängl, G., Giorgetta, M., & Brdar, S. (2015). Large eddy simulation using the general circulation model ICON. *Journal of Advances in Modeling Earth Systems*, *7*, 963–986. https://doi.org/10.1002/2015MS000431

Dorrestijn, J., Crommelin, D. T., Siebesma, A. P., & Jonker, H. J. J. (2013). Stochastic parameterization of shallow cumulus convection estimated from high-resolution model data. *Theoretical and Computational Fluid Dynamics*, *27*(1), 133–148. https://doi.org/10.1007/s00162-012-0281-y

Durran, D. R., & Weyn, J. A. (2016). Thunderstorms do not get butterflies. *Bulletin of the American Meteorological Society*, *97*(2), 237–243.

Heinze, R., Dipankar, A., Henken, C. C., Moseley, C., Sourdeval, O., Trömel, S., et al. (2017). Large-eddy simulations over Germany using ICON: A comprehensive evaluation. *Quarterly Journal of the Royal Meteorological Society*, *143*(702), 69–100.

Hong, S.-Y., & Dudhia, J. (2012). Next-generation numerical weather prediction: Bridging parameterization, explicit clouds, and large eddies. *Bulletin of the American Meteorological Society*, *93*(1), ES6–ES9. https://doi.org/10.1175/2011BAMS3224.1

Klocke, D., & Rodwell, M. (2014). A comparison of two numerical weather prediction methods for diagnosing fast-physics errors in climate models. *Quarterly Journal of the Royal Meteorological Society*, *140*(679), 517–524.

Lander, J., & Hoskins, B. J. (1997). Believable scales and parameterizations in a spectral transform model. *Monthly Weather Review*, *125*(2), 292–303. https://doi.org/10.1175/1520-0493(1997)125<0292:BSAPIA>2.0.CO;2

LeMone, M. A., Chen, F., Tewari, M., Dudhia, J., Geerts, B., Miao, Q., et al. (2010). Simulating the IHOP_2002 fair-weather CBL with the WRF-ARW-NOAH modeling system. Part II: Structures from a few kilometers to 100 km across. *Monthly Weather Review*, *138*, 745–764.

Miller, A. (2000). Alan Miller's Fortran software. Retrieved from https://jblevins.org/mirror/amiller/random.f90

Neggers, R. A. J., Köhler, M., & Beljaars, A. C. M. (2009). A dual mass flux framework for boundary layer convection. Part I: Transport. *Journal of the Atmospheric Sciences*, *66*(6), 1465–1487. https://doi.org/10.1175/2008JAS2635.1

Palmer, T. N. (2001). A nonlinear dynamical perspective on model error: A proposal for non-local stochastic-dynamic parametrization in weather and climate prediction models. *Quarterly Journal of the Royal Meteorological Society*, *127*(572), 279–304.

Piotrowski, Z. P., Smolarkiewicz, P. K., Malinowski, S. P., & Wyszogrodzki, A. A. (2009). On numerical realizability of thermal convection. *Journal of Computational Physics*, *228*, 6268–6290.

Plant, R. S., & Craig, G. C. (2008). A stochastic parameterization for deep convection based on equilibrium statistics. *Journal of the Atmospheric Sciences*, *65*, 87–105.

Sakradzija, M., & Hohenegger, C. (2017). What determines the distribution of shallow convective mass flux through a cloud base? *Journal of the Atmospheric Sciences*, *74*(8), 2615–2632. https://doi.org/10.1175/JAS-D-16-0326.1

Sakradzija, M., Seifert, A., & Dipankar, A. (2016). A stochastic scale-aware parameterization of shallow cumulus convection across the convective gray zone. *Journal of Advances in Modeling Earth Systems*, *8*, 786–812. https://doi.org/10.1002/2016MS000634

Sakradzija, M., Seifert, A., & Heus, T. (2015). Fluctuations in a quasi-stationary shallow cumulus cloud ensemble. *Nonlinear Processes in Geophysics*, *22*, 65–85. https://doi.org/10.5194/npg-22-65-2015

Seifert, A., & Beheng, K. (2006). A two-moment cloud microphysics parameterization for mixed-phase clouds. Part 1: Model description. *Meteorology and Atmospheric Physics*, *92*(1-2), 45–66.

Siebesma, A. P., Soares, P. M. M., & Teixeira, J. (2007). A combined eddy-diffusivity mass-flux approach for the convective boundary layer. *Journal of the Atmospheric Sciences*, *64*(4), 1230–1248. https//doi.org/10.1175/JAS3888.1

Sommeria, G., & Deardorff, J. W. (1977). Subgrid-scale condensation in models of nonprecipitating clouds. *Journal of the Atmospheric Sciences*, *34*(2), 344–355. https://doi.org/10.1175/1520-0469(1977)034<0344:SSCIMO>2.0.CO;2

Takemi, T., & Rotunno, R. (2003). The effects of subgrid model mixing and numerical filtering in simulations of mesoscale cloud systems. *Monthly Weather Review*, *131*, 2085–2101.

Tiedtke, M. (1989). A comprehensive mass flux scheme for cumulus parameterization in large-scale models. *Monthly Weather Review*, *117*(8), 1779–1800.

Zängl, G., Reinert, D., Rípodas, P., & Baldauf, M. (2015). The ICON (icosahedral non-hydrostatic) modelling framework of DWD and MPI-M: Description of the non-hydrostatic dynamical core. *Quarterly Journal of the Royal Meteorological Society*, *141*(687), 563–579.

Zhou, B., Simon, J. S., & Chow, F. K. (2014). The convective boundary layer in the terra incognita. *Journal of the Atmospheric Sciences*, *71*, 2545–2563.